A False-alarm-controllable Modified AdaBoost Wake Detection Method Using SAR Images

Yanan Guan, Huaping Xu, *Member, IEEE*, Wei Liu, *Senior Member, IEEE*, Chunsheng Li
Yuheng Liu

***Abstract*— A false-alarm-controllable modified AdaBoost based method is proposed for detecting ship wake from sea clutter in synthetic aperture radar (SAR) images. It reformulates the wake detection problem as a binary classification task in the multi-feature space. The update strategy of the sample weights in the original AdaBoost is modified for wake detection. First, a detection result confidence factor is designed to deal with class imbalance between sea clutter and ship wake; then, the AdaBoost is further modified as a false alarm rate (FAR) controllable detector by introducing penalty parameters to adjust weights update strategies for the sea clutter. Meanwhile, the multi-feature space is spanned by a novel frequency peak height ratio (FPHA) feature and four salient features. FPHA is proposed to enhance separation between the wake and sea clutter, which is computed from the amplitude spectrum peak of the image after Fourier transform. Experimental results show that the proposed detector can tackle the imbalanced data problem and flexibly control FAR by adjusting penalty parameters. Moreover, improved detection probability is also achieved compared with existing methods.**

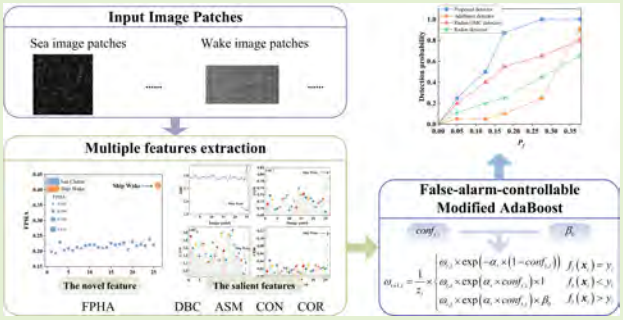

***Index Terms*—wake detection, SAR image, machine learning, SAR features, sea clutter.**

I. Introduction

SYNTHETIC aperture radar (SAR) plays a dominant role in microwave remote sensing due to its wide observation range, high spatial resolution and all-weather and all-day availability [1][2]. As an application of SAR imaging, wake detection is an important problem in marine environment monitoring [3]. Compared with ship hull detection, it is more advantageous to detect ship's wake pattern. For example, the wake can extend over several kilometers and a long period of time in SAR images [4], and it is more reflective of some important motion parameters of a ship, such as speed, size and heading [5]. However, the detection performance degrades with varying sea clutter and noise.

There have been many studies for ship wake detection through identifying the straight lines from speckle noise and the sea clutter background, since the wake pattern displays edge-like linear structures [6][7], i.e., bright or dark lines. As a result, single line feature based detectors are developed for ship wakes in the transform domain, such as Radon transforms (RT) and Hough transforms (HT) [8][9]. Most of them are based on RT, since it can reduce the effect of noise or sea clutter [10]. To improve the performance, some image processing methods are incorporated into the RT-based technique [9]. In [11], Rey et al. used the mean high-pass filter as a preprocessing step to increase the signal-to-noise ratio (SNR), and the Wiener filter as a post-processing step to reduce the probability of false alarm (PFA), while Kuo et al. presented a wavelet correlator to extract wake edges [12]. However, a low signal-to-clutter ratio may prevent these methods from obtaining satisfactory detection results [8]. Recently, compressive sensing and sparse representation have been employed in sea clutter suppression and wake detection [13]-[15]. They model SAR images as sea clutter plus wake and noise, separate them from each other, and then detect wake by RT [13]. Biondi employed the low-rank component plus sparse decomposition in both image domain and Radon domain to separate sea clutter in [14]. Oktay et al. treated wake detection as an inverse problem with sparse generalized minimax concave (GMC) penalty to support decision information in the Radon domain [4]. Nevertheless, these detectors have enhanced line representation to improve the robustness of wake detection, but it is still difficult to tackle the wake detection problem because some sea wave components are similar to the wake and the single line feature is rather limited in wake detection [3].

The ship wake in SAR images is a mixture of multiple components, including Kelvin wake, narrow V-wake, turbulent wake, and internal wake [4][7][16], and its pattern displays different grayscale intensities from the sea surface [17], which means that different wake patterns own individual textural information. So, multiple features based on the intensity and texture can provide more discriminability between wake and sea clutter [18][19].

As a multiple feature-based detector, AdaBoost has been one

This work was supported by the National Natural Science Foundation of China under Grant U2241202. *(Corresponding author: Huaping Xu)*

Yanan Guan, Huaping Xu, Chunsheng Li and Yuheng Liu are with the School of Electronic and Information Engineering, Beihang University, Beijing 100191, China (e-mail: xuhuaping@buaa.edu.cn).

Wei Liu is with the School of Electronic Engineering and Computer Science, Queen Mary University of London, E1 4NS London, U.K.

of the most successful machine learning algorithms, due to its high accuracy and efficiency in SAR image target detection [20]-[25]. AdaBoost iteratively updates sample weights, trains a series of base classifiers based on them, and linearly integrates these classifiers as a strong detector. The sample weights update strategy enables AdaBoost to focus on the samples that are difficult to classify. Based on this, the integrated strong detector has a better accuracy than the corresponding base classifiers. Sun [20] proposed an AdaBoost-based model to distinguish three types of ground vehicles in the MSTAR database. Fan et al. [21] combined AdaBoost and a CNN for feature augmentation and applied it to SAR images for ten-class vehicle detection. Moreover, AdaBoost is less prone to overfitting than other supervised machine learning models, particularly for small samples [24].

Ship wake detection in SAR images is a classic small-sample task, since the acquisition of wake is difficult [16]. Inspired by this, the AdaBoost detector is introduced for ship wake detection utilizing multiple features. However, there are two challenges when directly applying AdaBoost to wake detection. Firstly, class imbalance between sea clutter and wake pattern always exists and the amount of the latter is much smaller than the former. The detection accuracy under imbalanced data will be biased towards the majority—sea clutter and affect correct detection of the minority—the wake [26] Secondly, the current AdaBoost method fails to consider FAR controllability for a stable detection performance [27], which is necessary for wake detection. To address the above two challenges, a modified AdaBoost method for SAR wake detection is proposed in this paper. The main contributions of the proposed method are as follows:

1. A detection result confidence factor is proposed in sample weighting strategies to deal with the imbalanced data. The confidence factor can slow down the rate of weight update and modify the AdaBoost to guarantee the wake detection accuracy.
2. A penalty parameter is further introduced in sample weighting strategies to design a false-controllable AdaBoost. It flexibly controls the FAR by adjusting weights of the misclassified sea clutter.
3. The multi-feature space is explored to enhance separation between the wake and sea clutter, which is spanned by a novel feature in frequency, FPHA, and four salient features.

By applying the multi-feature space to the modified AdaBoost, a novel ship wake detector is proposed. Experimental results are provided to demonstrate the effectiveness of the proposed method.

The remainder of this paper is organized as follows. Section II briefly presents the basic work. The description of the proposed detection method is in Section III. Finally, experimental results and conclusions are provided in Section IV and Section V, respectively.

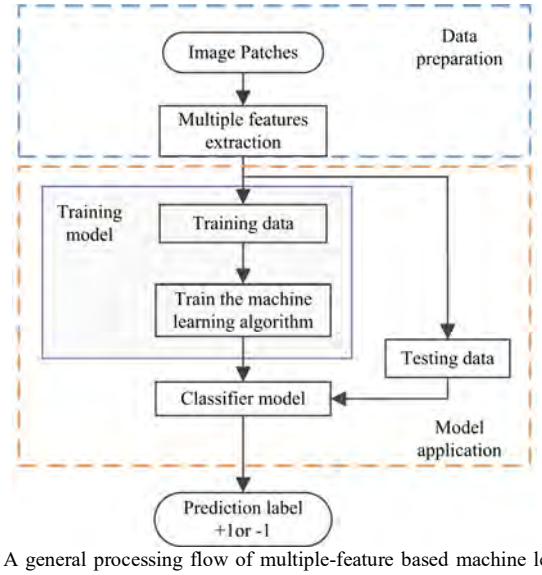

Fig.1. A general processing flow of multiple-feature based machine learning classifier.

II. BASIC WORK

Most ship wake detectors are carried out by RT on the basis of the single linear structure of wake in SAR images. The resultant detection performance is likely to be affected by the complex sea surface background. Thus, it is worthy to explore multiple-feature based ship wake detector [28]. In this section, the basic concept of wake detection and AdaBoost are introduced.

A. The ship wake detection problem

SAR image target detection can be essentially formulated as a binary classification problem [28], which discriminates the region of interest as a target class or a clutter class. The ship wake is a specific kind of SAR image target and a SAR image can also be considered as a sum of the wake pattern component and the sea clutter and noise component. Thus, wake detection can be formulized as the following binary hypothesis classification problem:

$$\begin{cases} \mathrm{H}_0 : I = s \\ \mathrm{H}_1 : I = s + w \end{cases} \tag{1}$$

where, the input of the binary hypothesis test is a series of image patches cut from SAR images, I is one of the image patches under test (IPUT), and the null hypothesis H_0 is for the absence of wake pattern in the IPUT. The alternative hypothesis H_1 denotes the presence of wake pattern in the IPUT. For the other notations, s refers to the sea clutter plus noise component in the IPUT, and w is the wake pattern component.

As a result, multiple-feature based classifier can be used to improve ship wake detection in the complex sea surface. Machine learning based classifiers have been very effective in tackling the classification task in a multi-feature space. A general classification flow based on machine learning [29] can be summarized in Fig. 1, which contains three parts. The first part is data preparation, where the images are cut into small patches which are further divided to training data and testing data. The second part is classifier model training, where the features are extracted from the image patches to construct a

multi-feature space which is then used as input to train the classifier. The third part is model application, where the trained model is applied to predict the label for testing data. So, the effective multi-feature space and the classifier model are two key parts for ship wake detection. This paper tries to explore some discriminative features and develop a SAR image ship wake detector based on multiple-feature machine learning.

B. AdaBoost

AdaBoost is a representative classifier in machine learning. It trains a series of base classifiers by iteratively updating the weights of samples, and linearly combines these base classifiers into a more effective one to obtain the boosted classification result [30]. AdaBoost focuses on the misclassified samples and assigns large weights for them to decrease classification errors, while small weights are assigned for the correctly classified samples. Except for the first base classifier, other classifiers in sequence are trained by the assigned weights that change in the iteration process. Thus, update strategy of the sample weights directly affects the classification result [31].

For a binary classification task, training data is composed of N samples, i.e., $(\boldsymbol{x}_1, y_1), \ldots, (\boldsymbol{x}_i, y_i) \ldots, (\boldsymbol{x}_N, y_N)$ $i = 1, 2, \ldots N$, where $\boldsymbol{x}_i$ is an input sample and $y_i \in (-1, +1)$ is the class label of $\boldsymbol{x}_i$. The sample with target is the positive sample, while the others without target are the negative ones. At the beginning of AdaBoost, the sample weights can be initialized by $\omega_{1,i} = 1/N$, and the iteration number is set as T. Then, sample weights are updated at the $t+1$ iteration as

$$\omega_{t+1,i} = \frac{1}{z_t} \times \begin{cases} \omega_{t,i} \times \exp(-\alpha_t) & f_t(\boldsymbol{x}_i) = y_i \\ \omega_{t,i} \times \exp(\alpha_t) & f_t(\boldsymbol{x}_i) \neq y_i \end{cases}, \tag{2}$$

where, $\omega_{t,i}$ is the weight of the i^{th} sample at the $t^{th}, (t = 1, 2, \cdots, T)$ iteration step, and $z_t = \sum \omega_{t,i}$ is the normalized factor. α_t is the coefficient of the t^{th} base classifier $f_t(\boldsymbol{x})$, and represents the importance of $f_t(\boldsymbol{x})$.

After T iterations, the strong classifier $F(\boldsymbol{x})$ is constructed by T base classifiers as:

$$F(\boldsymbol{x}) = sign\left(\sum_{t=1}^{T} \alpha_t f_t(\boldsymbol{x})\right), \tag{3}$$

where,

$$\alpha_t = \frac{1}{2} \ln \frac{1 - e_t}{e_t} \tag{4}$$

$sign(\cdot)$ is the sign operator defined as,

$$sign\left(\sum_{t=1}^{T} \alpha_t f_t(\boldsymbol{x})\right) = \begin{cases} 1 & \sum_{t=1}^{T} \alpha_t f_t(\boldsymbol{x}) \geq 0 \\ -1 & \sum_{t=1}^{T} \alpha_t f_t(\boldsymbol{x}) < 0 \end{cases}$$

and e_t is the training error of $f_t(\boldsymbol{x})$ given by

$$e_t = \sum_{i=1}^{N} \omega_{ti} In\left(f_t(\boldsymbol{x}) \neq y_i\right), \tag{5}$$

with $In(\cdot)$ being an indicator function as defined below

$$In\left(f_t(\boldsymbol{x}) \neq y_i\right) = \begin{cases} 1, & f_t(\boldsymbol{x}) \neq y_i \\ 0, & f_t(\boldsymbol{x}) = y_i \end{cases}.$$

As such, the smaller the classification error e_t of $f_t(\boldsymbol{x})$, the larger its importance coefficient α_t. The AdaBoost in (3) outputs $+1$ or -1 to predict the classification result for the input sample.

However, there are two challenges for AdaBoost's application in ship wake detection. The first one is class imbalance and the second one is related to false alarm control. The objective of machine learning is to minimize the errors [27]; for this purpose, the weight update strategy in (2) increases the weights of the misclassified samples while decreases that of the correctly classified samples. The weight of a misclassified sample is increased by $e^{\alpha_t} / e^{-\alpha_t} = e^{2\alpha_t}$ relative to a correctly classified sample. If one sample is repeatedly misclassified, the increase of its weight will be exponential, and the weights of other correctly classified samples will be exponentially decreased. Then, the base classifiers focus too much on these misclassified samples with large weights, and ignore samples that are correclty classified in the previous iteration steps. It means that large change of sample weights between the adjacent iterations will decrease the accuracy of the final strong classifier $F(\boldsymbol{x})$ [26].

In addition, facing class imbalance, AdaBoost tends to be biased towards the majority class in order to decrease the classification error [32]. As such, the weights of majority class samples have rapid rate of expansion and the peroformance may be poor for the minority class with rapidly shrinking weights, even indentified as noise [32]. In fact, the minority class generally serves as targets of interest with the positive label $+1$, and as such, class imblance can lead to a further decrease in the accuray of AdaBoost classification.

What's more, the weight update strategy in (2) only considers whether the classification result of a sample is correct or wrong, rather than whether the wrong sample is wake or sea clutter. However, SAR image target detection requires different penalties for misclassified clutter and wake [33], which demands a tighter control over the PFA than the detection probability. It may perform poorly on ship wake since it lacks in FAR controllability in supporting a stable detection performance [34].

III. Ship Wake Detector Based on FAR-Controllable Modified AdaBoost

In this section, the modified false-alarm-rate-controllable AdaBoost for wake detection is developed. The FAR-controllable modified AdaBoost is proposed by introducing a detection result confidence factor to deal with class imbalance and the penalty parameter to achieve controllability of FAR. To enhance the separation between sea clutter and ship wake in SAR images, a multi-feature space is constructed, which consists of a novel feature, FPHA and four salient existing features.

A. FAR-controllable modified AdaBoost

1) Detection Result Confidence Factor

Ship wake detection is a typical example for the class imbalance problem. Thus, it is important for AdaBoost to slow down the rate of weight update to improve detection accuracy.

The weights $\omega_{t+1,i}$ at the $(t+1)^{th}$ iteration obviously depend on the previous classification result of $f_t(\boldsymbol{x})$; however, the result may be unreliable [26], leading to misclassification again at the next iteration, since the weights will be updated significantly based on an unreliable result. As stated previously, these repeated misclassifications will bring about rapid exponential change of sample weights, which affects the classification accuracy of the final classifier $F(\boldsymbol{x})$. An intuitive solution is to incorporate a reliable constraint into (2), on which the rate of weight update is slowed down. For example, if a sample has been misclassified many times in previous iterations, which indicates the sample is quite difficult for detector to identify, then a large increase should be made into the weights for the current iteration; while if a sample has been correctly classified many times in previous iterations, a slow increase in the weights is required on the premise that AdaBoost pays attention to the misclassified samples. All results of previous t iterations can indicate a confidence level whether it is necessary to give a larger weight for the misclassified samples. However, the classification results of previous t iterations are not taken into account in the weight update strategy in (2), where only the last result is considered. Therefore, a detection result confidence factor is defined and introduced into the sample weight update strategy as follows.

The confidence $conf_{t,i}$ is defined as the ratio of the number of times that the i^{th} sample is misclassified in previous $t(t \le T-1)$ iterations to the total number of iterations

$$conf_{t,i}(\boldsymbol{x}) = \frac{\sum_{m=1}^{t} In\left(f_m(\boldsymbol{x}_i) \ne y_i\right) + \varepsilon}{T}. \tag{6}$$

And the update strategy in (2) can be reformulated as:

$$\omega_{t+1,i} = \frac{1}{z_t} \times \begin{cases} \omega_{t,i} \times \exp\left(-\alpha_t \times \left(1 - conf_{t,i}\right)\right) & f_t(\boldsymbol{x}_i) = y_i \\ \omega_{t,i} \times \exp\left(\alpha_t \times conf_{t,i}\right) & f_t(\boldsymbol{x}_i) \ne y_i \end{cases}, \tag{7}$$

where $\sum_{m=1}^{t} In\left(f_m(\boldsymbol{x}_i) \ne y_i\right)$ denotes the total number of misclassified times of one sample in previous iterations. ε is a positive parameter to avoid the case of $conf_{t,i} = 0$. If $conf_{t,i} = 0$ in (7), the part $\omega_{t,i} \times \exp(\alpha_t \times 0) = \omega_{t,i}$ fails to adjust weights for the misclassified samples. So, we set $\varepsilon = 1$ and then $conf_{t,i}(\cdot) \in \left[\frac{1}{T}, 1\right]$ is a positive parameter. Due to the error of a base classifier should be $e_t > 0.5$ [30], α_t in (4) is also positive; considering the exponential is a monotonically inceasing function, $\exp\left(\alpha_t \times conf_{t,i}\right) < \exp(\alpha_t)$ and the value $\exp\left(\alpha_t \times conf_{t,i}\right)$ increases more slowly with the number of misclassified times.

Similarly, $\left(1 - conf_{t,i}\right) \in \left[0, \frac{T-1}{T}\right]$ is also a positive parameter, and $\exp(-\alpha_t)$ is a monotonically decreasing function.

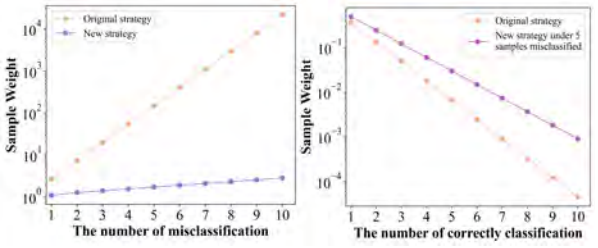

(a) (b)

Fig. 2. Comparison of weight update strategies for (a) misclassification, and (b) correct classification.

Since $\alpha_t \times \left(1 - conf_{t,i}\right) < \alpha_t$, larger weights can be obtained as $\exp\left(-\alpha_t \times \left(1 - conf_{t,i}\right)\right) > \exp(-\alpha_t)$, compared with that in (2). The part of $\exp\left(-\alpha_t \times \left(1 - conf_{t,i}\right)\right)$ decreases more slowly with the number of correctly classified times. As a result, $conf_{t,i}$ curbs the speed of change in sample weights.

To illustrate the effect of $conf_{t,i}$, a comparison of sample weights between (2) and (7) is provided. The sample weights are calculated for the wrong classification and correct classification, respectively. For simplicity, $\omega_{t,i}$ and α_t are not considered here, as the positive parameters have little influence on the trend of the weight update process. Then, the weights can be simplified as $\exp\left(-1 \times \left(1 - conf_{t,i}\right)\right)$ and $\exp\left(conf_{t,i}\right)$. The iteration number is set as $T = 20$. For misclassification, suppose one sample has been misclassified 10 times continuously from the beginning; for correct classification, suppose one sample has been correctly classified 10 times continuously after 5 misclassifications. The corresponding sample weights in a logarithmic scale with respect to the classification number are plotted in Fig. 2(a) and 2(b). It is shown that the weight given by the original update strategy increases or decreases rapidly, while that of the proposed method is much slower. It indicates that $conf_{t,i}$ can indeed slow down the rate of weight update while still following the AdaBoost principle as stated.

For the class imbalance problem, the proposed $conf_{t,i}$ can curb the weight update rate and guarantee a suitable weight for wake sample.

2) Penalty parameters for FAR controllability

Although the weight determined by (7) is slowed down to guarantee the wake detection accuracy, the issue of uncontrollable false alarm is still not taken into consideration in this strategy. It only considers whether the classification result of a sample is correct or not, rather than whether the wrong sample is wake or sea clutter. However, SAR image target detection requires different penalties for misclassified clutter and target [33], which demands a tighter control over the PFA than the detection probability. AdaBoost may perform poorly on ship wake since it lacks FAR controllability, which is important for a stable detection performance [34].

Furthermore, in practice, a detector should be able to obtain a better result with controllable false alarms, where the misclassification of background is restricted with a given false

alarm probability, while the accuracy for targets permits an acceptable compromise. However, according to (7), the base classifier only focuses on the classification result, not considering the result of each target or background. Thus, penalty parameters are introduced to control misclassification for background and target, and the weight update strategy can be further modified as:

$$\omega_{t+1,i}=\frac{1}{z_t}\times\begin{cases}\omega_{t,i}\times\exp\left(-\alpha_t\times\left(1-conf_{t,i}\right)\right) & f_t\left(\boldsymbol{x}_i\right)=y_i\\ \omega_{t,i}\times\exp\left(\alpha_t\times conf_{t,i}\right)\times\beta_1 & f_t\left(\boldsymbol{x}_i\right)<y_i\\ \omega_{t,i}\times\exp\left(\alpha_t\times conf_{t,i}\right)\times\beta_0 & f_t\left(\boldsymbol{x}_i\right)>y_i\end{cases}, \quad (8)$$

From (8), increasing β_1 for a given β_0 can reduce misclassification of targets and increase FAR, since the weight of the misclassified target samples is increased in this case. Similarly, increasing β_0 for a given β_1 can reduce the misclassification of background and decrease FAR. However, a practical detection task normally requires a better detection result with a lower false alarm rate; then, the weight update strategy in FAR-controllable modified AdaBoost is designed as

$$\omega_{t+1,i}=\frac{1}{z_t}\times\begin{cases}\omega_{t,i}\times\exp\left(-\alpha_t\times\left(1-conf_{t,i}\right)\right) & f_t\left(\boldsymbol{x}_i\right)=y_i\\ \omega_{t,i}\times\exp\left(\alpha_t\times conf_{t,i}\right)\times 1 & f_t\left(\boldsymbol{x}_i\right)<y_i\\ \omega_{t,i}\times\exp\left(\alpha_t\times conf_{t,i}\right)\times\beta_0 & f_t\left(\boldsymbol{x}_i\right)>y_i\end{cases}. \quad (9)$$

From (9), the FAR can be flexibly controlled by adjusting β_0. A set of dataset is employed to demonstrate how the parameter β_0 affects the FAR. The dataset is taken from sklearn [35], to serve as an example of linear non-separable data with Gaussian noise. A detailed introduction is presented in Section IV. Here, two categories of data with labels $\{+1,-1\}$ are generated and contain 10000 samples, respectively. Three different iteration numbers T are set. For each T, a series of FARs of the modified AdaBoost are calculated under different β_0 values ranging from 1 to 3. This process is repeated under three different values of T. The FAR is defined as

$$P_F=\frac{\text{The number of misclassified negative samples}}{\text{The total number of negative sampels}}. \quad (10)$$

The results are shown in Fig. 3. It displays that FAR varies with β_0, and a larger β_0 corresponds to a smaller FAR. The FAR of a larger T is smaller for the same β_0. Hence, the proposed weight update strategy can embed FAR into AdaBoost and flexibly control it by adjusting the penalty parameter β_0.

The pseudocode for the proposed FAR-controllable modified AdaBoost method is provided in Table I, where the involved learning procedure is performed in two phases after initialization.

In the first phase (Lines 3–10), it is iteratively trained with a fixed iteration number T. The actual P_F is calculated based on the trained method. In the second phase (Lines 11–16), a bisection method is used to adjust β_0 by comparing the calculated P_F to the required value P_f where the upper and lower bounds of β_0 are set at the initialization part.

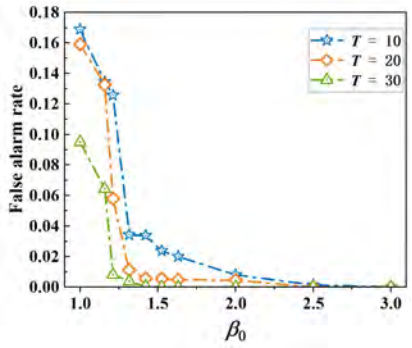

Fig. 3. FAR versus different β_0 under different iteration number.

TABLE I
ALGORITHM FOR FAR-CONTROLLABLE MODIFIED ADABOOST

Algorithm 1: A FAR-controllable modified AdaBoost

1: **Initialization**:
Set base classifier $f\left(\boldsymbol{x}\right)$: decision tree stump,
Set the FAR P_f and the threshold η=0.0001 ,
$\beta_0=1, P_F=1; upper=3, lower=1$.
2: **While** $\left|P_F-P_f\right|>\eta$ **do**:
3: **Iteration**: $t=1,2,\ldots,T$.
4: Fit a base classifier: $f_t\left(\boldsymbol{x}\right):\boldsymbol{x}\rightarrow\left(+1,-1\right)$.
5: Calculate the error for base classifier using (5).
6: Calculate the coefficient of base classifier using (4).
7: Calculate the confidence parameters $conf_{t,i}$ using (6).
8: Calculate and update the sample weights using (9).
9: Construct a strong classifier using (3).
10: Calculate the FAR using (10).
11: **If** $P_F=P_f$ **then**: Break
12: **Else if** $P_F>P_f$ **then:**
$lower=\beta_0, \beta_0=\frac{upper+lower}{2}$.
13: **Else if** $P_F<P_f$ **then:**
$upper=\beta_0, \beta_0=\frac{upper+lower}{2}$.
14: **End if**
15: **End while**
16: **Output** $F\left(\boldsymbol{x}\right)=sign\left(\sum\alpha_i f_i\left(\boldsymbol{x}\right)\right)$.

The above procedure is then repeated until the difference between P_F and P_f is no more than a set threshold and at the end the final strong classifier $F\left(\boldsymbol{x}\right)$ is obtained.

B. Multi-feature space for wake detection

Multiple features can provide sufficient difference between target and background from different perspectives, so multiple features are applied for ship wake detection here instead of a linear structural feature. In particular, the FPHA feature is proposed and forms the multi-feature space by combining with the other four discriminative features, which are differential box counting (DBC), energy (ASM), contrast (CON), and correlation (COR). Furthermore, the separability of wake and sea clutter in these features is analyzed.

1) FPHA

The grayscale intensity variations in a SAR image are intuitively associated with frequencies through Fourier transform. The zero-frequency term is proportional to the

average energy of an image. For an intensity-smooth image, the slow varying grayscale intensity corresponds to low frequencies, and the energy in the frequency domain is concentrated on these low frequencies; a fast intensity change, such as edges or textures of objects, corresponds to high frequencies, and therefore the energy expands into these high frequency components. The sea SAR image appears dark, since the reflection coefficient of sea surface is low. The grayscale intensity variation is slow, and the energy is mainly focused on low frequencies. However, there are edges and textures in wake regions, so the energy spreads to high frequency too. An example of sea and wake in a SAR image and its histogram are respectively shown in Fig. 4 (a) and Fig. 4(b). It can be seen that the grayscale intensity of sea clutter is more concentrated than that of wake. The energy distribution of sea clutter and wake in the frequency domain is shown in Fig. 5. Compared with sea clutter, the energy of wake has a tendency towards high frequencies, so the energy difference in the frequency domain can be a discrimination feature to separate the wake from sea clutter.

To enhance and quantify this difference, the FPHA is proposed. First, the two-dimensional FFT amplitude spectrum of I is calculated by

$$\left|F(u,v)\right| = \left|\sum_{x=0}^{M-1}\sum_{y=0}^{N-1} I(m,n)\exp\left(-j2\pi\left(\frac{um}{M}+\frac{vn}{N}\right)\right)\right|, \tag{11}$$

where, $I(m,n)$ denotes the grayscale intensity at the pixel (m,n) of I. Then, the histogram of 2-D amplitude spectrum $\left|F(u,v)\right|$ is calculated and denoted as $\mathrm{H}(\cdot)$. The height of the peak in $\mathrm{H}(\cdot)$ is represented as $\mathrm{PH}(\cdot)$ and the peak corresponds to the frequency amplitude A. Then, the FPHA is defined as

$$\mathrm{FPHA}(I) = \frac{\mathrm{PH}\left(\mathrm{H}\left(\left|F(u,v)\right|\right)\right)}{A}. \tag{12}$$

As the wake energy is distributed over more frequency components, the corresponding amplitude A is smaller than that of sea clutter.

The frequency amplitude spectrum histograms of two image patches taken from Fig. 4(a) are shown in Fig. 6, where the logarithm of amplitude is employed to show more details. It can be found that the PH of wake is higher than that of sea clutter and the corresponding A is smaller than that of sea clutter. So the proposed feature is larger for wake than for sea clutter. To further illustrate its validity, a real SAR image is cut into 25 sea clutter patches and one wake patch, and the FPHAs of these 26 image patches are calculated and shown in Fig. 7. For notational simplicity, these 25 clutter patches are indexed from #1 to #25, and the wake patch is labeled as #26. It is shown that the wake FPHA is indeed larger and the proposed FPHA can distinguish the wake from the sea clutter effectively.

2) DBC

The fractal model has been widely employed to represent the irregularity of natural object surface and analyze image characteristics in tasks such as target detection and recognition. Sea clutter can be established as a typical kind of fractal geometry, due to the complexity and irregularity of the rough

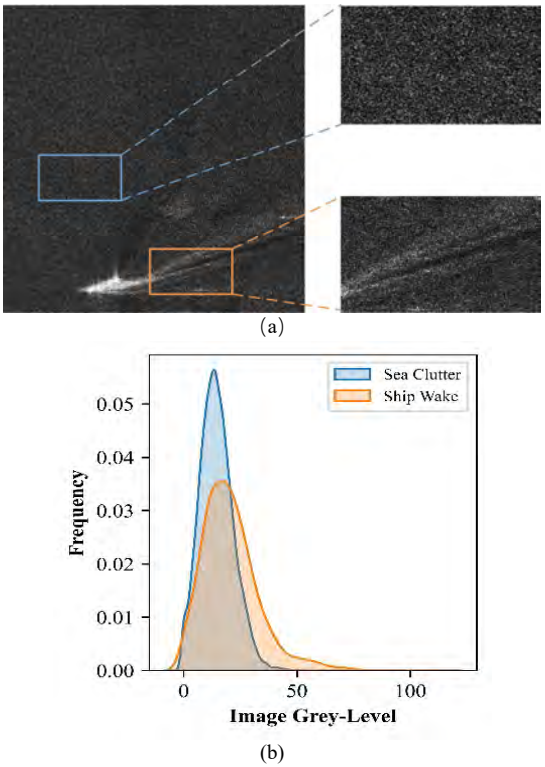

Fig 4. Illustration of grayscale SAR image textures difference between sea clutter and wake: (a) an example of real ship wake SAR image; (b) the histograms of sea clutter (blue box) and ship wake (orange box) regions in (a).

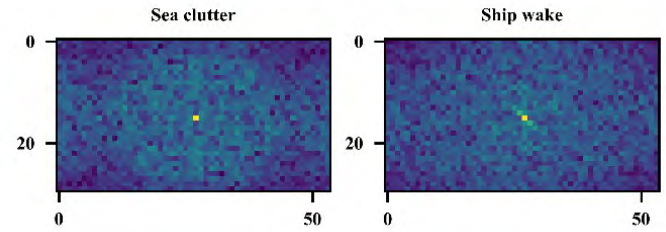

Fig.5. Energy contrast of the sea clutter and wake patches from Fig. 4(a) in the frequency domain.

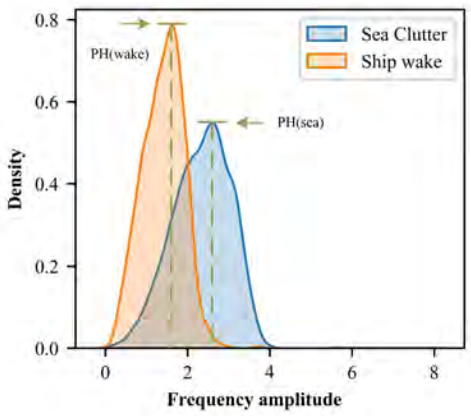

Fig.6. Histogram contrast of the distribution of sea clutter and wake in the image frequency amplitude spectrum operated by log, and the FPHAs of wake and sea clutter are 0.53 and 0.21, respectively.

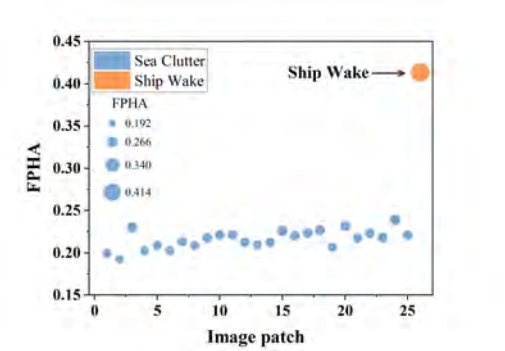

Fig. 7. FPHA features for 26 SAR image patches from HRSID (P0005_1800_2600_5400_6200). The first 25 circles correspond to FPHAs of sea clutter image patches and the last one represents FPHA of wake image features (marked with an arrow); the larger the circle, the higher the FPHA.

sea surface. As an effective fractal feature, differential box counting is extracted from the patches and successfully used to distinguish targets from sea clutter in SAR images [36]. In this process, DBC serves as a textual feature to supply additional information for SAR image ship wake detection.

A SAR image patch I with size $M\times N$ can be considered as a three-dimensional surface, where the third dimension corresponds the grayscale of I. Then, some boxes of integer size $s\times s\times s$ ($1\le s\le \min(M/2, N/2)$) are used to cover I, and the number of these boxes is $N_s = l-k+1$, i.e., the distance between the highest box (l) and the lowest box (k). The fractal dimension of I is measured as

$$\mathrm{DBC}_s = \frac{\log(N_s)}{\log(1/s)}. \tag{13}$$

Adjust the size of each box and obtain a set of fractal dimensions $(s_1, N_{s1}),\cdots(s_k, N_{sk})$. Then, the DBC feature of patch I is measured by fitting these fractal dimensions in the least squares sense.

3) Texture features for the gray-level co-occurrence matrix (GLCM)

GLCM is an important tool for evaluating SAR image texture features in target detection. Specifically, ASM, CON, and COR have been demonstrated to be more effective GLCM-based features for improved detectability and discriminability. These three textural features were extracted and calculated using a sliding window of 5×5 pixels as follows:

$$\mathrm{ASM} = \sum_{m,n} p(m,n)^2, \tag{14}$$

$$\mathrm{CON} = \sum_{m,n} (m,n)^2 p(m,n), \tag{15}$$

$$\mathrm{COR} = \sum_{m,n} \frac{(m-\mu_m)(n-\mu_n)p(m,n)}{\sigma_m\sigma_n}. \tag{16}$$

where $p(m,n)$ is the GLCM entry at (m,n), and

$$\mu_m = \sum_{m,n} mp(m,n)$$

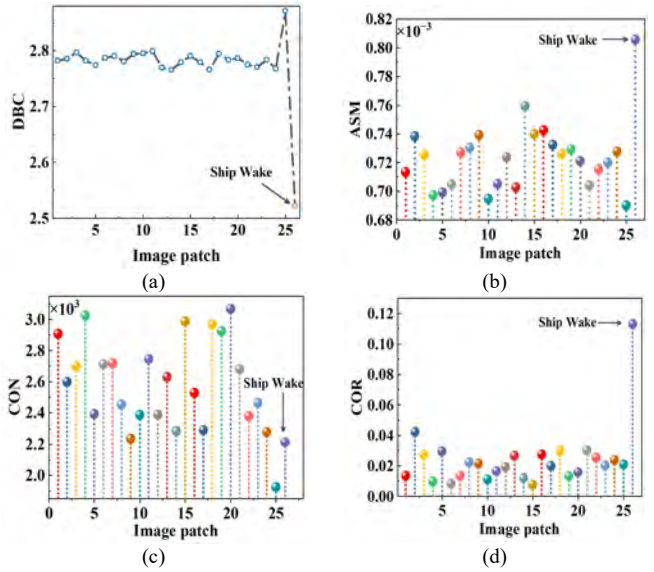

Fig. 8. Textural features for 26 SAR image patches from HRSID (P0005_1800_2600_5400_6200). The first 25 points in each plot correspond to sea clutter image patch features and the last point represents wake image features (marked with an arrow). Individual plots also show (a) the DBC, (b) the ASM, (c) the CON, and (d) the COR of patches.

$$\mu_n = \sum_{m,n} np(m,n)$$

$$\sigma_n = \sqrt{\sum_{i,j}(m-\mu_m)^2 p(m,n)} \quad \sigma_n = \sqrt{\sum_{i,j}(m-\mu_m)^2 p(m,n)}$$

The DBC, ASM, CON as well as COR of 26 image patches are estimated and plotted in Fig. 8. The four features show the separability of ship wake and sea clutter. It is evident that the IPUT with sea clutter-only exhibits a larger DBC than that of the wake patch in Fig. 8(a), which demonstrates significant DBC discriminability of sea clutter and wake patterns. ASM denotes the uniformity of object textural information; the higher the ASM, the more regular the texture is. So ship wakes exhibit a larger value than that of sea clutter in Fig. 8(b). CON assesses local variations as shown in Fig. 8(c). If there is a large grayscale difference in IPUT, the CON feature takes on a larger value. Since the grayscale of the wake changes gradually, the ship wake will have a smaller CON. There is a small overlap between CON of sea clutter and that of wake when sea surface is calm and its grayscale changes slowly. COR describes the similarity of objects in some direction for IPUT. The COR of 26 image patches is provided in Fig. 8(d). Considering the wake pattern has its own clear textures, the COR of wake is prominently larger than that of sea clutter. The above five features exhibit sufficient separability between sea clutter and wake, and they are also capable of reflecting the differences between the sea clutter and wake from multiple perspectives. Although the contribution made by the CON feature may be small, it helps with enhancing the detection performance to some extent.

C. Proposed detector based on FAR-controllable modified AdaBoost

For the FAR-controllable modified AdaBoost, the SAR image patches are completely represented by the constructed multi-feature space.

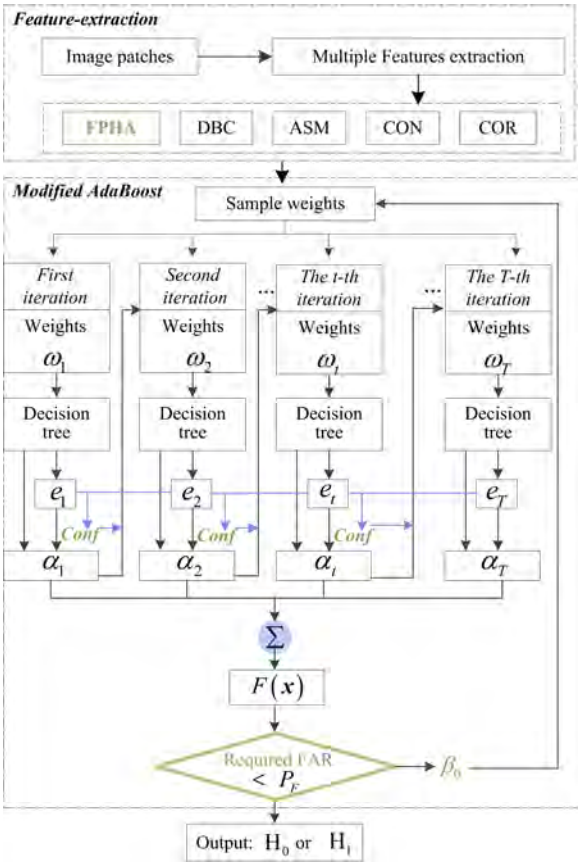

Fig 9. Block diagram of the proposed detector based on FAR-controllable modified AdaBoost, including dataset construction, wake detector training and testing.

Using the multi-feature space in section III. B, the detector based on FAR-controllable modified AdaBoost is proposed for SAR wake detection and the procedure is shown in Fig. 9 and composed of three steps.

Firstly, each SAR image is cut into small patches as in Fig. 1, and five features are extracted from them forming a feature space to represent SAR images, which are employed as input to train the detector. The sea clutter feature space $\mathbf{X}_{sea}=\{\boldsymbol{x}_{sea1},\boldsymbol{x}_{sea2},\cdots,\boldsymbol{x}_{seai},\cdots\boldsymbol{x}_{seaN}\}$ is extracted from N sea clutter IPUTs, where $\boldsymbol{x}_{seai}$ denotes the i^{th} sea clutter sample, expressed by,

$$\boldsymbol{x}_{seai}=\left[\mathrm{FPHA}(s_i),\mathrm{DBC}(s_i),\mathrm{ASM}(s_i),\mathrm{CON}(s_i),\mathrm{COR}(s_i)\right]^T$$

The size of the ship wake feature space is smaller than that of sea clutter, with $\mathbf{X}_{wake}=\{\boldsymbol{x}_{wake1},\boldsymbol{x}_{wake2},\cdots,\boldsymbol{x}_{wakei},\cdots\boldsymbol{x}_{wakeM}\}$, which is extracted from M ship wake IPUTs and $\boldsymbol{x}_{wake}=\left[\mathrm{FPHA}(w_i),\mathrm{DBC}(w_i),\mathrm{ASM}(w_i),\mathrm{CON}(w_i),\mathrm{COR}(w_i)\right]^T$ denotes the i^{th} ship wake sample. These feature samples are input to train the modified AdaBoost. Secondly, the parameter $conf_{t,i}$ is introduced into the weight to deal with the class imbalance problem as shown Table I. Finally, FAR is calculated and compared with a required P_f. If the difference is larger than the threshold, then adjusting the penalty parameter and reaptedly traing model until meet the threshold.

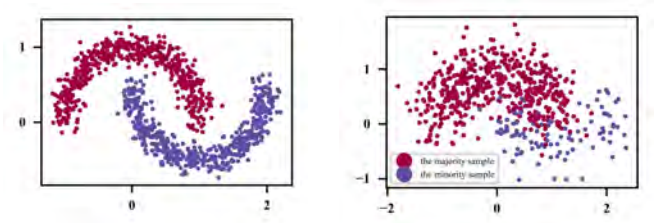

Fig. 10. Examples of the generated simulation data: (a) a balance example; (b) example of an imbalance ratio of 1:5.

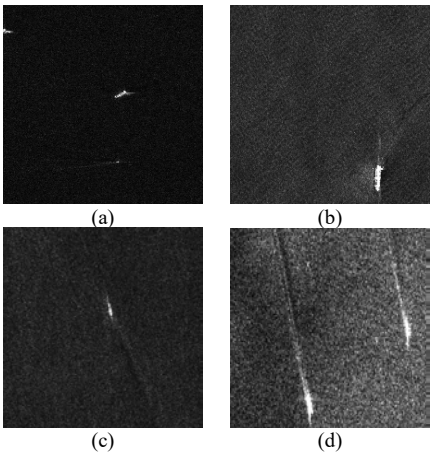

Fig. 11. Examples of real SAR images: the first row shows images from HRSID; the second row are from SSDD.

IV. Experimental Results

In this section, firstly, effectiveness of the proposed $conf_{t,i}$ for the modified AdaBoost is investigated with respect to the minority class detection accuracy in the imbalance problem; secondly, controllability of FAR for the modified AdaBoost is further explored; finally, the ship wake detection performance by the modified AdaBoost method is compared with some existing ones.

Simulated data and real SAR images are utilized to validate the proposed method, respectively. To facilitate visualization, the simulated data, as shown in Fig. 10, is given as an example for 2-D linearly non-separable dataset with Gaussian noise, which satisfies the linearly indivisibility property between the wake and sea clutter. The data consists of positive samples and negative samples. The positive samples ($+1$) denote presence of wake patterns as the minority class, while the negative samples (-1) is for sea clutters, as the majority class. For the first two perspectives, the experiments require sufficient linearly non-separable data to verify the method's effectiveness. Hence, the simulated data are utilized in Section IV-A and in Section IV-B.

The real SAR images, as shown in Fig. 11, are chosen from the open-access HRSID data [38] and SSDD data [39]. They are mainly acquired from RadarSat-2, Sential-1B and TerraSAR-X with four fundamental polarization states—HH, VV, HV, and VH. The resolution of SSDD data ranges from 1m to 15m, while that of HRSID is 0.5m, 1m and 3m. The HRSID data is used as the training data and the SSDD dataset as the test data, which can also examine the generalization ability of the multi-feature space constructed in this work. During

pre-processing, these SAR images are cut into image patches with appropriate sizes.

A. Experimental Results for Class Imbalance

To assess the detection performance of the modified AdaBoost for class imbalance, some evaluation criteria are utilized, which are defined on binary classfication confusion martix shown in Table II. TP is the number of positive samples correctly classified, and FP is the number of misclassified negtive samples that are considered as false alarm samples; FN is the number of misclassified positive samples, and the TN is the number of negative samples correctly classified.

Based on the confusion matrix, three evaluation criteria, widely used to evaluate the detection performance of class imbalance [32] are defined as:

$$P_D = \frac{\mathrm{TP}}{\mathrm{TP+FN}}$$

$$P_F = \frac{\mathrm{FP}}{\mathrm{FP+TN}}$$

$$\mathrm{F1} = 2 \times \frac{\mathrm{Precision} \times P_D}{\mathrm{Precision} + P_D}$$

where, $\mathrm{Precision} = \mathrm{TP}/(\mathrm{TP+FP})$ and the detection probability P_D measures the ability of detector to identify positive samples. The higher P_D is, the more positive samples are identified. The false alarm probability P_F reflects the ability of detector to correctly predict positive samples. The lower P_F is, the higher the accuracy of the detector. For the class imbalance problem, the size of the positive samples is usually small, i.e. TN is larger than TP. It may lead to a lower P_F and lower P_D. F1 considers accuracy and identification ability together. The higher the F1, the better the performance of the detector. Thus, P_D, P_F and F1 are considered in the following to evaluate the detection results. All of them range from 0 to 1.

Meanwhile, the detection ability is tested and compared with AdaBoost [38] under different imbalance conditions to demonstrate the modified AdaBoost effect with class imbalance. To illustrate the imbalance degree, the imbalance ratio b is defined as

$$b = N_{minority} / N_{majority}$$

where $N_{minority}$ is the number of the minority samples (wake samples), and $N_{majority}$ is the number of majority class samples (sea clutter samples). Then, a series of simulated data are generated with different b between the positive samples and negative ones. The data is divided into two parts. One part is used to train AdaBoost and the modified AdaBoost; the other is for the testing.

For the training, the size of the simulated data with the minority class is set as 400. Based on the size of the minority class, the size of the majority class is set according to the imbalance ratio index b, which varies from 1:4 to 1:10. The minority class and majority class are labeled as $\{+1, -1\}$, respectively. The distribution of the testing data is the same as that of the training data. But the size of the minority class is set as 100, and b remains the same. For every b, the experiment with the modified AdaBoost and AdaBoost is repeated 10 times. The result is evaluated by P_D, P_F and F1 every time. And the average of the three criteria in 10 times is calculated, respectively. The curves of average P_D, P_F and F1 varying with b are plotted in Fig. 12(a)-(c). It is shown in Fig. 12(a) that the modified AdaBoost has a higher P_D than AdaBoost, which indicates that the introduced parameter, $conf(x)$ can slow down the update rate of the weight and then improve the identification ability for the minority class. As shown in Fig. 12(b) and Fig. 12(c), the false alarms of the modified AdaBoost are slightly larger than AdaBoost, while F1 of the modified AdaBoost is higher than AdaBoost. The increase of P_D will result in the loss of P_F [26]. In comparison with AdaBoost, increase of P_D by the modified AdaBoost is larger than the increase of P_F. This indicates that the proposed modified AdaBoost can improve detection accuracy of the minority class for the imbalance problem.

TABLE II
A CONFUSION MATRIX OF BINARY CLASSIFICATION

	The prediction class	
The actual class	Positive	Negative
Positive	TP	FN
Negative	FP	TN

TABLE III
A CONTROLLABILITY COMPARISON FOR TRAINING DATA AND TESTING DATA

	P_f	Training dataset (10000 samples)		Testing dataset (2500 samples)	
		False	P_F	False	P_F
The proposed AdaBoost	0.1	962	0.0962	251	0.1004
	0.01	95	0.0095	23	0.0092
	0.001	10	0.001	4	0.0016
AdaBoost	/	983	0.0983	250	0.1000

B. Experimental Results for False Alarm Controllability

To verify the FAR controllability of the modified AdaBoost, balanced data is generated to avoid the influence of imbalanced samples on flexible control of FAR. The average FAR at the training stage is compared with that at the testing stage under three different values of P_f —(0.1, 0.01, 0.001). For each P_f, 12500 samples are generated for each class, and it is divided into training and testing data as $(10000, 2500)$.

For a given P_f, the training process of the modified AdaBoost is implemented by Algorithm 1 and the FAR is calculated by (10). Then, the testing data is input into the trained modified AdaBoost and the FAR of the detection result is calculated. The above process is repeated 10 times; the average FARs, P_F, are listed in Table III in comparison with those of AdaBoost. It can be seen that the original AdaBoost fails to consider FAR and it cannot be controlled to get close to the required P_f; however, FARs achieved by the modified AdaBoost are close to the given P_f, which demonstrates that modified AdaBoost can control the FAR effectively.

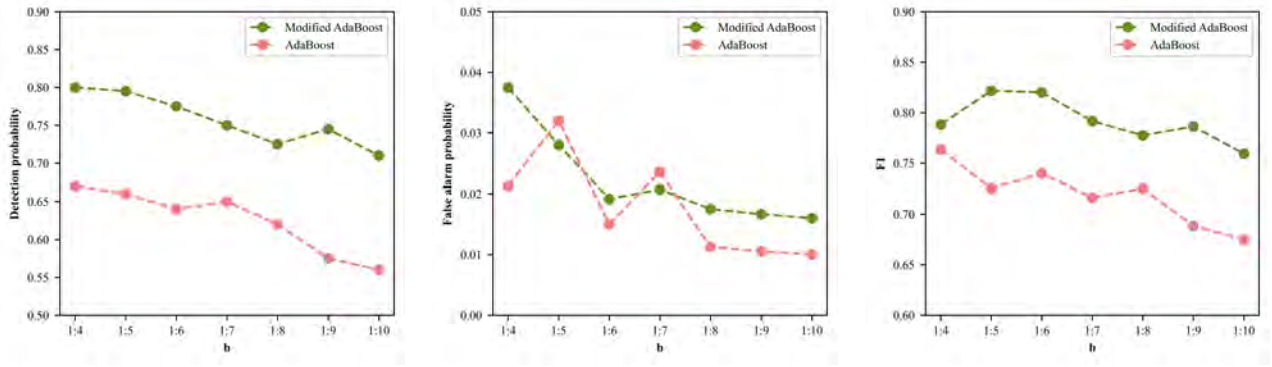

Fig. 12. Detection results by the modified AdaBoost and AdaBoost based on the simulated data for (a) P_D , (b) P_F , and (c) F1 under different b

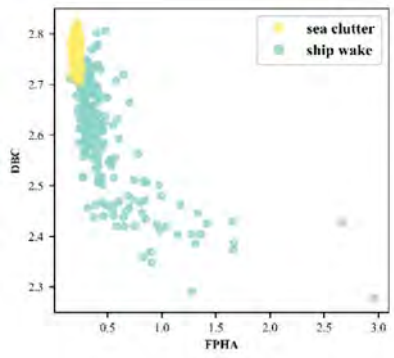

Fig. 13. Distribution of sea clutter and ship wake on FPHA and RPH.

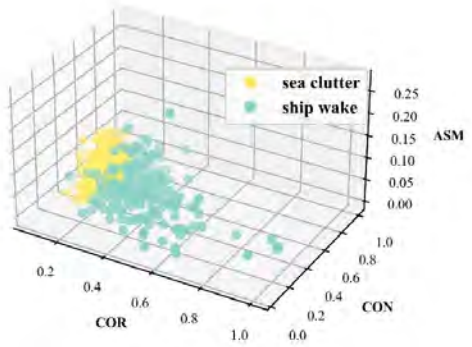

Fig. 14. Scatter distribution of sea clutter and ship wake in the 3-D feature space.

C. Ship Wake Detection

To verify the ship wake detection performance, experiments based on the FAR-controllable modified AdaBoost-based detector are carried out via real SAR images. These SAR images are divided into training data and testing data. In the training process, 228 wake image patches as target and 2500 sea clutter patches as background are obtained from the HRSID database. In the testing process, 40 wake image patches as target and 450 sea clutter patches as background are collected from the SSDD dataset. These image patches cover different sea states, polarization modes and satellite platforms. In addition, the training data and the testing data come from different publicly available dataset; the diversity of data can be adopted to test the effectiveness and generalization of the extracted features and the proposed detector.

According to the block diagram in Fig. 9 and Fig. 1, the training and testing data is first prepared for the extraction of five features. For visualization, the FPHA and DBC features are combined, and their distribution is shown in the 2-D space in Fig. 13, while the other three features i.e., ASM, CON and COR are drawn together in the 3-D space in Fig. 14. It can be seen that there is obvious discriminability between sea clutter and ship wake in the five-feature space. After feature extraction, the detector is trained. In experiment, the base classifier is set as a decision tree stump that utilizes the Gini index [33] to classify these features. According to[33], a smaller Gini index implies a higher accuracy, and all the features can be divided by selecting the minimum Gini index. Here, the iteration number is set as $T = 20$ .The modified AdaBoost-based wake detector combines these 20 decision tree stumps linearly into as a strong wake detector.

Then, the modified AdaBoost-based detector is compared with AdaBoost[30], Radon with GMC [4] and Radon [16] using the testing data. Some detection results using the ship wake image patches from SSDD are shown in Fig. 15. The correctly detected patches are labelled with red box. The SAR image patches are listed in the first column, and the results by the modified AdaBoost are listed in the second column, while the results by AdaBoost, Radon with GMC and Radon are presented in the third, the fourth and the fifth columns. The results of the two AdaBoost-based detectors are better than those of RT-based ones. As shown, it is difficult for RT based methods to detect wake edges that are weak in contrast to the sea clutter. The results indicate that the constructed multiple-feature space is effective and can offer more information to aid the detection. Moreover, the results also show that the proposed detector based on FAR-controllable modified AdaBoost outperforms than the others.

The detection probabilities, P_D , of the four detectors are calculated and compared under a set of different FARs for the testing data. The curves of detection probability and FARs are

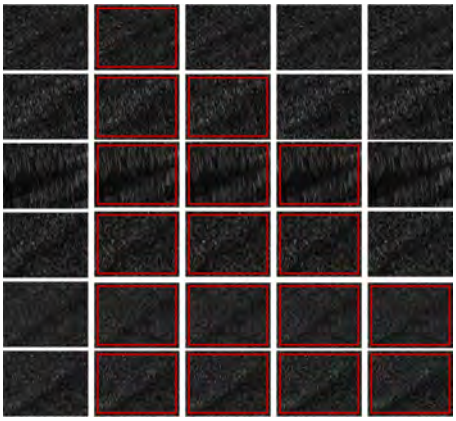

Fig. 15. Some examples for the ship wake detection results. The first column is the original image patches from SSDD, and the second, third, fourth and final columns respectively show the results of the modified AdaBoost, AdaBoost, Radon with GMC and Radon; the correctly detected patches are labeled with red box.

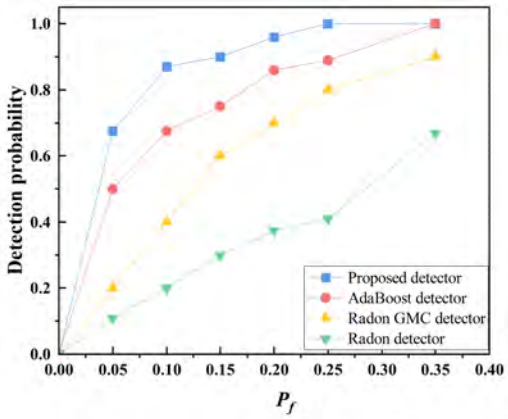

Fig. 16. Detection probabilities with various FARs for different detectors

shown in Fig. 16. It is obvious that the P_D value of all detectors increases with the increase of FAR, and the multi-feature based detectors perform better than Radon-based methods, with the proposed method using the constructed multi-feature space always giving the best result. When the FAR is 0.1, the detection probability of the proposed detector is about 0.87, while that of AdaBoost is 0.675. And the detection probability of Radon with GMC is 0.4 and that of Radon is 0.2.

V. Conclusions

In this paper, a novel modified AdaBoost-based wake detector with multi-feature space has been proposed. The proposed method can improve the wake detection performance under various SAR images, which overcomes the limitation of single-feature based detection. In particular, a detection result confidence factor is proposed in the sample update strategy to deal with class imbalance between ship wake and sea clutter. Then, a penalty parameter is also introduced in the sample update strategy to flexibly control FAR of the detector. By adding a novel FPHA feature, the multi-feature space is constructed to enhance the separability between ship wake and sea clutter. As demonstrated by experimental results, the proposed method can improve the wake detection probability with a given false alarm probability for real SAR image data, compared with the existing detectors.

In the future, multi-scale and more meaningful features, such as multifractal features, could be explored and added in our detector to further improve its adaptability.

Appendix

The list of explanations for the important mathematical symbols used is displayed as follows. The symbols in the table are sorted according to the order in which they appear in the paper.

TABLE IV
AN EXPLANATIONS LIST OF IMPORTANT MATHEMATICAL SYMBOLS

Symbols	Description
FAR	False alarm rate
$\boldsymbol{x}_i$	Input sample
y_i	Label for input sample
T	Total number of AdaBoost iterations
ω	Sample weight
$f(\cdot)$	Base classifier
α_t	Coefficient of base classifier
$F(\cdot)$	AdaBoost output of the strong classifier
$sign(\cdot)$	Sign operator
e_t	Error for the base classifier
$In(\cdot)$	Indicator function
$conf_{t,i}$	Proposed confidence factor
β_0	Penalty parameter adjusting FAR
P_F	False alarm rate
P_f	Required false alarm rate

References

[1] X. Sun, P. Liu and Y. Q. Jin, "Ship Wake Components: Isolation, Reconstruction, and Characteristics Analysis in Spectral, Spatial, and TerraSAR-X Image Domains," *IEEE Trans. Geosci. Remote Sens.*, vol. 56, no. 7, pp. 4209-4224, July 2018.

[2] J. Li, L. Wang, M. Zhang, Y. -C. Jiao and G. Liu, "Ship Velocity Automatic Estimation Method Via Two-Dimensional Spectrum Pattern of Kelvin Wakes in SAR Images," *IEEE J. Sel. Topics Appl. Earth Observ. Remote Sens.*, vol. 14, pp. 4779-4786, 2021.

[3] A. Fujimura, A. Soloviev, S. H. Rhee and R. Romeiser, "Coupled Model Simulation of Wind Stress Effect on Far Wakes of Ships in SAR Images," *IEEE Trans. Geosci. Remote Sens.*, vol. 54, no. 5, pp. 2543-2551, May 2016.

[4] O. Karakuş, I. Rizaev and A. Achim, "Ship Wake Detection in SAR Images via Sparse Regularization," *IEEE Trans. Geosci. Remote Sens.*, vol. 58, no. 3, pp. 1665-1677, March 2020.

[5] A. C. Copeland, G. Ravichandran and M. M. Trivedi, "Localized Radon transform-based detection of ship wakes in SAR images," *IEEE Trans. Geosci. Remote Sens.*, vol. 33, no. 1, pp. 35-45, Jan. 1995.

[6] M. D. Graziano, M. D'Errico and G. Rufino, "Ship heading and velocity analysis by wake detection in SAR images", *Acta Astronaut.*, vol. 128, pp. 72-82, 2016.

[7] K. Ding, J, Yang J, Z. Wang, et al., Specific windows search for multi-ship and multi-scale wake detection in SAR images. *Remote Sens.*, vol. 14, no. 1, Dec. 2021.

[8] F. Biondi, "Low-Rank Plus Sparse Decomposition and Localized Radon Transform for Ship-Wake Detection in Synthetic Aperture Radar Images," *IEEE Geosci. Remote Sens. Lett.*, vol. 15, no. 1, pp. 117-121, Jan. 2018.

[9] F. Xue, W. Jin, S. Qiu, and J. Yang, "Rethinking automatic ship wake detection: State-of-the-art CNN-based wake detection via optical images," *IEEE Trans. Geosci. Remote Sens.*, vol. 60, pp. 1–22, 2022.

[10]P. Courmontagne, “An improvement of ship wake detection based on the radon transform,” *Signal Process*., vol. 85, no. 8, pp. 1634–1654, 2005.
[11]M. T. Rey, J. K. Tunaley, J. T. Folinsbee, P. A. Jahans, J. A. Dixon and M. R. Vant, "Application Of Radon Transform Techniques To Wake Detection In Seasat-A SAR Images," *IEEE Trans. Geosci. Remote Sens*., vol. 28, no. 4, pp. 553-560, July 1990,
[12]J. M. Kuo and K. S. Chen, “The application of wavelets correlator for ship wake detection in SAR images,” *IEEE Trans. Geosci. Remote Sens.*,vol. 41, no. 6, pp. 1506–1511, Jun. 2003.
[13]Y.-H. Zhao, X. Han, and P. Liu, “A RPCA and RANSAC based algorithm for ship wake detection in SAR images,” in Proc. 12th Int. Symp. Antennas, Propag. *EM Theory (ISAPE)*, Dec. 2018, pp. 1–4.
[14]F. Biondi, "A Polari metric extension of low-rank plus sparse decomposition and radon transform for ship wake detection in synthetic aperture radar images," *IEEE Geosci. Remote Sens. Lett*., vol. 16, no. 1, pp. 75-79, Jan. 2019.
[15]G. Yang, J. Yu, C. Xiao, and W. Sun, “Ship wake detection for SAR images with complex backgrounds based on morphological dictionary learning,” P*roc. IEEE Int. Conf. Acoust., Speech Signal Process.(ICASSP)*, Mar. 2016, pp. 1896–1900 .
[16]G. Zilman, A. Zapolski, and M. Marom, “On detectability of a ship’s Kelvin wake in simulated SAR images of rough sea surface,” *IEEE Trans. Geosci. Remote Sens*., vol. 53, no. 2, pp. 609–619, Jun. 2014.
[17]J. K. E. Tunaley, E. H. Buller, K. H. Wu and M. T. Rey, "The simulation of the SAR image of a ship wake", *IEEE Trans. Geosci. Remote Sens*., vol. 29, no. 1, pp. 149-156, Jan. 1991.
[18]Z. Sun et al.,” An anchor-free detection method for ship targets in high-resolution SAR images,” *IEEE J. Sel. Topics Appl. Earth Observ. Remote Sens.*, vol.14, pp. 7799-7816, 2021.
[19]B.Xiong and Z.Sun et al.,” A lightweight Model for Ship Detection and Recognition in Complex-Scene SAR images,” *Remote Sens*.,14(23), 6053, Nov. 2022.
[20]Y. Sun, Z. Liu, S. To dorovic and J. Li, "Adaptive boosting for SAR automatic target recognition," *IEEE Trans. Aerosp. Electron. Syst*., vol. 43, no. 1, pp. 112-125, January 2007.
[21]F. Zhang, Y. Wang, J. Ni, Y. Zhou and W. Hu, "SAR Target Small Sample Recognition Based on CNN Cascaded Features and AdaBoost Rotation Forest," *IEEE Geosci. Remote Sens. Lett.*, vol. 17, no. 6, pp. 1008-1012, June 2020.
[22]J. Ai, R. Tian, Q. Luo, J. Jin, and B. Tang, “Multi-scale rotation invariant Haar-like feature integrated CNN-based ship detection algorithm of multiple-target environment in SAR imagery,” *IEEE Trans. Geosci. Remote Sens.*, vol. 57, no. 12, pp. 10070–10087, Dec. 2019.
[23]C. P. Schwegmann, W. Kleynhans and B. P. Salmon, "Synthetic aperture radar ship detection using Haar-like features", *IEEE Geosci. Remote Sens. Lett*., vol. 14, no. 2, pp. 154-158, Feb. 2017.
[24]J. Yang et al, “No-reference quality assessment for screen content images using visual edge model and AdaBoosting neural network,” *IEEE Trans. Image Process.*, vol.30, pp. 6801-6814, 2021.
[25]M. Mahrooghy, J. V. Aanstoos, R. A. A. Nobrega, K. Hasan, S. Prasad and N. H. Younan, "A Machine Learning Framework for Detecting Landslides on Earthen Levees Using Space borne SAR Imagery," *IEEE J. Sel. Topics Appl. Earth Observ. Remote Sens*., vol. 8, no. 8, pp. 3791-3801, Aug. 2015.
[26]W. Wang and D. Sun, “The improved AdaBoost algorithms for imbalanced data classification,” *Inf. Sci*. vol. 563, pp. 358-374, March 2021.
[27]Y. Li, P. Xie, Z. Tang, T. Jiang, and P. Qi, “SVM-based sea-surface small target detection: A false-alarm-rate-controllable approach,” *IEEE Geosci. Remote Sens. Lett*., vol. 16, no. 8, pp. 1225–1229, Aug. 2019.
[28]S. Xu, J. Zheng, J. Pu, and P. Shui, “Sea-surface floating small target detection based on polarization features,” *IEEE Geosci. Remote Sens.Lett*., vol. 15, no. 10, pp. 1505–1509, Oct. 2018
[29]X1. Microaneurysm detection in fundus image using small image patches and machine learning.
[30]J. Zhu, H. Zou, S. Rosset and T. Hastie, “Multi-class Adaboost,” *Statistics and Its Interface*, vol. 2, no. 1, pp. 349–360, 2009.
[31]S. Wu and H. Nagahashi, “Parameterized AdaBoost: introducing a parameter to speed up the training of real AdaBoost,” *IEEE Signal Process. Lett*., vol. 21, no. 6, pp. 687-691, June 2014.
[32]Y. Jiang, W. Xu, Y. Zhang, Q. Zhu and Y. He, “An Imbalanced Multifault Diagnosis Method Based on Bias Weights AdaBoost,” *IEEE Trans. Instrum. Meas*., vol. 71, pp. 1-8, March 2022.
[33]H. Zhou and T. Jiang, “Decision Tree Based Sea-Surface Weak Target Detection With False Alarm Rate Controllable,” *IEEE Signal Process. Lett*.,vol. 26, no. 6, pp. 793-797, June 2019.
[34]Q. Qu, Y.-L. Wang, W. Liu, and B. Li, “A false alarm controllable detection method based on CNN for sea-surface small targets,” *IEEE Geosci. Remote Sens. Lett*., vol. 19, pp. 1–5, 2022.
[35]P. Tiwari, S. Dehdashti, A. K. Obeid, “Kernel Method based on Non-Linear Coherent State”, arXiv preprint arXiv:2007.07887, 2020.
[36]C. Panigrahy, A. Seal, N. K. Mahato, and D. Bhattacharjee, “Differential box counting methods for estimating fractal dimension of gray-scale images: A survey,” *Chaos, Solitons Fractal*s, vol. 126, pp. 178–202, 2019.
[37]X. M. Li, Y. Sun and Q. Zhang, "Extraction of Sea Ice Cover by Sentinel-1 SAR Based on Support Vector Machine With Unsupervised Generation of Training Data," *IEEE Trans. Geosci. Remote Sens vol*. 59, no. 4, pp. 3040-3053, April 2021.
[38]S. Wei, X. Zeng, Q. Qu, M. Wang, H. Su, and J. Shi, “HRSID: A High-Resolution SAR images Dataset for Ship Detection and Instance Segmentation,” *IEEE Access*, vol.8, pp.120234-120254, 2020.
[39] J. Li, C. Qu, and J. Shao, “Ship detection in SAR images based on an improved faster R-CNN,” *Proc. BIGSARDATA*, Beijing, China, pp. 1–6, Nov. 2017.